

PREPARED FOR SUBMISSION TO JHEP

CAVENDISH-HEP-11/17

DCPT/11/84

IPPP/11/42

MAN/HEP/2011/13

## Identifying the colour of TeV-scale resonances

---

**S. Ask<sup>a</sup> J.H. Collins<sup>a</sup> J.R. Forshaw<sup>b</sup> K. Joshi<sup>b</sup> A.D. Pilkington<sup>b,c</sup>**

<sup>a</sup>*Cavendish Laboratory, University of Cambridge, Cambridge CB3 0HE, UK.*

<sup>b</sup>*School of Physics & Astronomy, University of Manchester, Manchester M13 9PL, UK.*

<sup>c</sup>*Institute of Particle Physics Phenomenology, University of Durham, Durham DH1 3LE, UK.*

**ABSTRACT:** We explore how the colour of any new TeV-scale resonances that decay into top quark pairs can be identified by studying the dependence of the observed cross-section on a central jet veto. To facilitate this study, colour octet resonance production was implemented in PYTHIA8 and colour singlet resonance production is simulated after minor modifications. We find that the colour of a 2 TeV resonance can be identified with  $10 \text{ fb}^{-1}$  of data at a centre-of-mass energy of 14 TeV for a wide range of couplings, but only if the uncertainty in the theoretical prediction is dramatically reduced from its current level.

---

## Contents

<b>1</b>	<b>Introduction</b>	<b>1</b>
<b>2</b>	<b>Implementation of a gluon resonance in Pythia8</b>	<b>3</b>
<b>3</b>	<b>Extracting the colour of a heavy resonance</b>	<b>4</b>
3.1	Simulation and event selection	4
3.2	Definition of the jet veto region and the gap-fraction	6
3.3	Extracting the signal from background	7
3.4	Extracting the colour	8
3.5	Effect of experimental and theoretical uncertainties	12
<b>4</b>	<b>Acknowledgments</b>	<b>12</b>
<b>A</b>	<b>Appendix</b>	<b>15</b>

---

## 1 Introduction

The goal of this paper is to illustrate how one can gain insight into the colour of any new TeV-scale resonance that might be produced at the LHC. In the case where a resonance is observed in the invariant mass spectrum of dijets, the resonance mass will swiftly be measured as will its spin. However, it will also be important to identify the colour charge of the resonance. Generally speaking, differently coloured resonances will generate a different spectrum of accompanying radiation and one should expect to exploit this difference in order to establish the colour of the resonance. This matter has been explored in some recent papers [1–4] and our purpose is to present a detailed feasibility study that makes quantitative statements about the potential of such a measurement at the LHC.

In this paper, we explore the associated radiation via the introduction of a jet veto. In particular, we compute the rate of resonance production subject to the constraint that there should be no jets (apart from those arising from the decay of the resonance) lying in the central region of rapidity with transverse momentum above some scale,  $Q_0$ . The variation of the cross section with  $Q_0$  contains important information on the colour of the resonance. The method of jet vetoing to probe the colour structure of new physics should have other important applications, for example in [5] it was demonstrated that one can extract the effective couplings of the Higgs boson to weak vector bosons and to gluons by measuring the veto-scale dependence in “Higgs plus dijet” events with a veto on any third jet lying between the primary jets. We therefore expect the method to have general utility.

Jet vetoing has a number of advantages which make it well suited to the task in hand. Experimentally, the systematic uncertainties are expected to be small if one focusses on

a “gap fraction” (i.e. the ratio of the cross section with a veto to that without). This expectation is born out by recent gap fraction measurements in dijet events at the LHC [6]. Apart from that, any attempt to identify the colour structure of new physics processes will be hindered by background and by pile-up. One can minimize sensitivity to background by using observables that are defined over the ensemble of events and which can therefore be corrected for background provided it can be subtracted statistically. The gap fraction is such an observable since it is a measure of the  $Q_0$  dependence of the signal cross section. Observables that are measured on an event-by-event basis would suffer from inevitable contamination from background processes. In the high-luminosity phase of the LHC, there will typically be more than 20 pile-up interactions overlaying the signal and any method used to extract the colour flow needs to be robust to this extra activity. The jet veto method will be robust against pile-up if  $Q_0$  is chosen to be large and/or the vetoed jets are within the acceptance of the inner tracking detectors, as discussed in Section 3.2.

It is possible to study the colour structure of events using other methods. One such possibility is jet scaling [4, 7], which uses the cross-section ratios,  $\sigma(n+1)/\sigma(n)$ , for specific jet multiplicities,  $n$ . The information contained in these ratios is very similar to that contained in the gap fraction and we do not discuss it any further here. Another possibility might be to exploit the structure of jets to probe the colour flow, e.g. the ‘jet pull’ [2]. This approach should yield important information, however it suffers from event-by-event contamination from background and the effect of pile-up would also need to be studied. We shall focus on the jet veto method in what follows, whilst acknowledging that other methods may have a role to play should a new resonance be observed at the LHC.

Resonant production of a new heavy gauge boson is the primary signal of new physics at hadron colliders in several extensions of the Standard Model (SM). One popular scenario is within the Randall-Sundrum (RS) model [8–10] where all the SM fields have access to the extra dimensional space. In this scenario, the lightest Kaluza-Klein (KK) excitations of the gauge bosons primarily decay into top quarks. There are several alternative scenarios within this RS framework which have attracted interest as candidates to resolve a number of issues with the SM, *e.g.* the gauge hierarchy problem [8], the fermion mass hierarchy [11–13], gauge coupling unification [14–17], providing a dark matter candidate [18, 19]. In addition, recent results on the forward-backward asymmetry in top pair events from the CDF and DØ experiments indicate a potential deviation from the SM expectation [20–23], which could be caused by a colour octet resonance with a mass around 2 TeV [24]. For these reasons, we have chosen to investigate how the veto-scale dependence can discriminate between a colour octet and a colour singlet resonance, both with a mass of 2 TeV and spin-1.<sup>1</sup>

The outline of the paper is as follows: In Section 2, we discuss a new implementation of heavy gluon resonances in the PYTHIA8 Monte Carlo event generator. In Section 3, we use this implementation to study the feasibility of identifying the colour of such a resonance at the LHC. We start from the assumption that a new resonance has been observed at the LHC in  $pp$  collisions at  $\sqrt{s} = 14$  TeV. We then show how to quantify the

---

<sup>1</sup>No other colour is possible if the resonance is to couple to quark–anti-quark pairs.

probability of successfully extracting the colour of the resonance. Finally, we discuss the limiting theoretical and experimental uncertainties associated with the measurement.

## 2 Implementation of a gluon resonance in Pythia8

We have implemented the heavy gluon resonance process within the Monte Carlo generator PYTHIA8 [25, 26]. The implementation assumes that the heavy gluon can only be produced by quarks, i.e.  $q\bar{q} \rightarrow \tilde{G} \rightarrow q\bar{q}$ . At tree-level, the suppression of any coupling to gluons is a consequence of the Landau-Yang theorem (for massless gluons and a heavy spin-1 resonance) [27, 28] and it has also been shown that the suppression persists at one-loop in the Bulk RS model [29]. We include interference with SM QCD  $2 \rightarrow 2$  production and allow for general couplings to quarks, in particular different couplings to left and right-handed states are permitted. Such chiral couplings have recently been discussed in connection with the forward-backward asymmetry ( $A_{FB}$ ) measurements at the Tevatron [30, 31]. A forward-backward asymmetry caused by the heavy gluon at leading-order requires an axial-vector coupling to both the initial and final state quarks. For this reason, such an asymmetry is not expected in the common RS models [32], where the light quark couplings are vector-like. However, such studies might be of interest in alternative models.

Although the implementation is generic, we shall continue to make reference to the most common RS models, where the KK gluon coupling to top quarks is significantly stronger than to the other flavours and the total width is therefore dominated by the width from decays into tops. The fact that the final state flavour is normally different from the initial state flavour has the consequence that the light-quark couplings approximately determine the production cross section whereas the top coupling fixes the total width. The  $b$ -quark coupling is often sufficiently small that it only weakly effects the width and cross section, we therefore restrict the parameter space by fixing  $g_v^b$  to either be zero or the reference RS model value [9] discussed below. The heavy gluon uses the particle id code 5100021 and its corresponding decay channels can be specified through the standard PYTHIA8 particle data scheme.

Specifically, the total production cross section is given by

$$\sigma(\hat{s}) = \frac{8\pi\alpha_S^2}{27}\hat{s}[\sigma_{SM} + \sigma_{KK} + \sigma_{int}] , \quad (2.1)$$

$$\sigma_{SM} = \frac{\beta_j A_j}{\hat{s}^2} , \quad (2.2)$$

$$\sigma_{KK} = \frac{((g_v^i)^2 + (g_a^i)^2)((g_v^j)^2\beta_j A_j + (g_a^j)^2\beta_j^3)}{(\hat{s} - m_{\tilde{G}}^2)^2 + \left(\hat{s}\frac{\Gamma_{tot}}{m_{\tilde{G}}}\right)^2} , \quad (2.3)$$

$$\sigma_{int} = \frac{2}{\hat{s}} \cdot \frac{g_v^i g_v^j (\hat{s} - m_{\tilde{G}}^2)\beta_j A_j}{(\hat{s} - m_{\tilde{G}}^2)^2 + \left(\hat{s}\frac{\Gamma_{tot}}{m_{\tilde{G}}}\right)^2} , \quad (2.4)$$

where the subscripts indicate the contributions from the SM and KK gluon amplitudes and their interference. In the above formulae  $g_v^{i/j}$  and  $g_a^{i/j}$  represent the vector and axial-vector couplings to the initial and final state quarks, with flavours  $i$  and  $j$ ; the couplings are all

relative to the strong coupling in accordance with [33]. The partonic centre-of-mass energy is denoted  $\hat{s}$  and the quantities  $\beta_j$  and  $A_j$  are defined via

$$\beta_j = \sqrt{1 - 4\frac{m_j^2}{\hat{s}}} , \quad (2.5)$$

$$A_j = 1 + 2\frac{m_j^2}{\hat{s}} . \quad (2.6)$$

The masses  $m_{\tilde{G}}$  and  $m_j$  correspond to the KK gluon (which we generally refer to as the “heavy gluon”) and final state quark masses and the total width is obtained by summing the partial widths:

$$\Gamma(\tilde{G} \rightarrow q_j \bar{q}_j) = \frac{\alpha_S \beta \sqrt{\hat{s}}}{6} [(g_v^j)^2 A_j + (g_a^j)^2 \beta^2] . \quad (2.7)$$

In addition to specifying the KK gluon mass, the program offers the possibility to assign separate values of the KK gluon coupling to light, bottom and top quarks. The most common RS models often predict different couplings to different helicity states and therefore the couplings can also be assigned separately for left-handed and right-handed quarks. Finally, the hard process is integrated within the PYTHIA8 framework of parton showers, underlying event activity, hadronisation and unstable particle decays. The implementation has been validated against results in the literature and it has been used to investigate characteristic features of a heavy colour octet: some of those results are presented and discussed in the appendix.

### 3 Extracting the colour of a heavy resonance

In this section, we investigate the feasibility of distinguishing a 2 TeV colour octet resonance from an otherwise identical colour singlet resonance by vetoing on additional jet activity outside the di-top system.

#### 3.1 Simulation and event selection

Events are generated using the PYTHIA8 implementation of heavy gluon resonance production, as discussed in Section 2. The couplings used for the gluon resonance are  $g_v^q = 0.2$ ,  $g_v^b = 0$  and  $g_v^t = 3.6$ . The mass chosen for this study is 2 TeV. The resulting cross section  $\times$  branching-ratio is 1.1 pb and the resonance width is  $\Gamma/M = 0.2$ . Purely vector couplings are assumed and interference with the SM contribution is ignored. Heavy photon production is simulated by changing the colour flow. Specifically, we replace the colour factors and  $\alpha_s \rightarrow e_q^2 \alpha_{em}$ , where  $e_q$  is the electric charge<sup>2</sup>. We also adjusted (i) the coupling of the heavy photon to light quarks to reproduce the production rate for the heavy gluon and (ii) the coupling of the heavy photon to top quarks in order to match the total width of the heavy gluon. The CTEQ5L parton distribution functions are used [34] with the default tune to the underlying event (UE) of version 8.130 (Tune1) [25]. Details of the UE tune are

---

<sup>2</sup>In other words, we assume that the heavy colour singlet couples like a true photon.

$\sum E_T$ (GeV)	$\delta_p$	$R_{CA}$	$\delta_r$
$E_T \leq 1000$	0.13	0.9	0.19
$1000 < E_T \leq 1600$	0.10	0.8	0.19
$1600 < E_T \leq 2600$	0.05	0.6	0.19
$E_T > 2600$	0.05	0.4	0.16

**Table 1.** Parameters of the top-tagging algorithm.  $R_{CA}$  is the distance parameter that is used in the Cambridge-Aachen jet finding algorithm. The distance parameter is defined on an event-by-event basis since it is dependent on the scalar summed  $E_T$  of all particles in the event. The parameters  $\delta_p$  and  $\delta_r$  are defined in [38].

not very important – the sensitivity to non-perturbative physics was tested by repeating the analysis, but with hadronisation and multiple parton interactions switched off. We observe that the change in the gap fraction is less than 2% and therefore conclude that the soft physics modelling is not a crucial component in determining the feasibility of this measurement.

The top quarks will be highly boosted and form a dijet topology and so the primary background will come from QCD  $2 \rightarrow 2$  scattering. We define  $t\bar{t}$  and light-jet backgrounds separately, the latter being defined with no top-quarks in the final state. In both cases, the SM background events were simulated using PYTHIA8. Top-jet candidates are identified using the FASTJET library [35–37] and the Johns Hopkins top-tagging algorithm [38] (the parameters of the top-tagging algorithm are listed in Table 1). The input to the algorithm are stable particles from the MC event record that have  $|\eta| < 4.9$ , i.e. within the fiducial acceptance of the LHC detectors (neutrinos are removed). The events are then required to contain two tagged top-jets, each of which has  $p_T > 400$  GeV, after which the cross section for heavy gluon production is 46.8 fb and for heavy photon production it is 31.4 fb. This difference demonstrates an interesting and important difference in the tagging efficiency for top quarks originating from differently coloured resonances. We have confirmed that this difference is not due to non-perturbative physics, in particular we confirm that the difference in tagging efficiency arises after the parton shower with hadronization/underlying event playing a small role. It follows that, should such a resonance be observed at the LHC, the measurement of the colour flow (using a method such as that presented here) will be crucial in determining the production cross section.<sup>3</sup> For both resonances, the top tagging is sufficient to reduce the background to a manageable level in the region of the resonance. Figure 1(a) shows the invariant mass distributions of the tagged top quarks for each type of signal and background process.

In order to compare like-for-like resonances, we make a further adjustment to the heavy photon cross section so that it is equal to the heavy gluon cross section after top tagging, i.e.  $\sigma_0 = 46.8$  fb. In our final analysis, all results will be presented for a range of values of the production cross section (i.e.  $\sigma_0$  is a baseline value).

<sup>3</sup>The use of jet substructure (e.g. see the review in [39]) should yield additional information regarding the colour of the resonance, assuming that the effects of background contamination and pile-up can be brought under control.

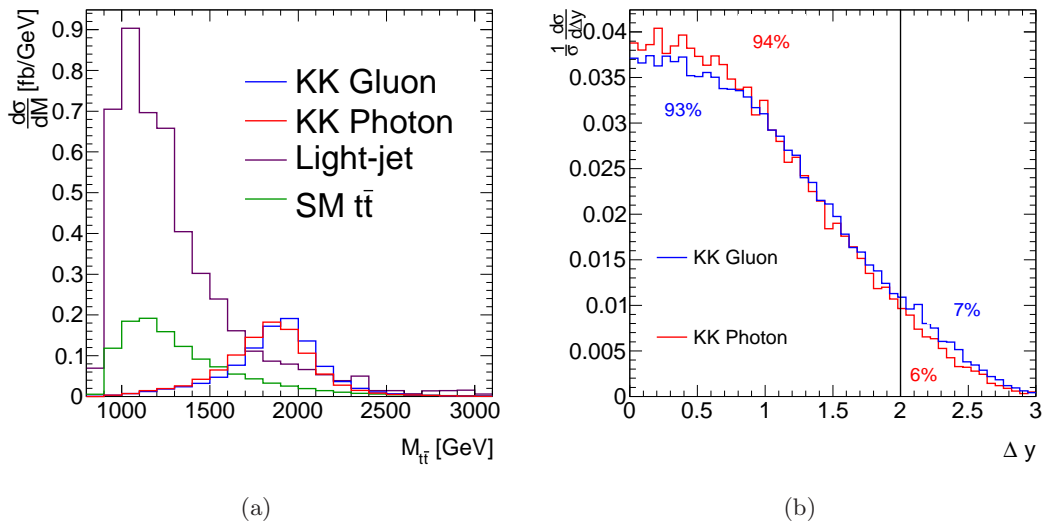


**Figure 1.** Signal and background distributions after tagging the two leading jets as top candidates. (a) The invariant mass of the top candidates. (b) The  $\Delta y$  between the top candidates.

### 3.2 Definition of the jet veto region and the gap-fraction

To identify the additional jet activity, we use the anti- $k_T$  algorithm with  $R = 0.6$ . The inputs to this second-stage jet finding are the full set of stable interacting particles, i.e. the same as to the top-tagging stage. We keep only those jets,  $j$ , that are sufficiently far in  $\eta - \phi$  space from the previously tagged top jets,  $t$ , i.e.

$$\Delta R = (\Delta\eta_{j,t}^2 + \Delta\phi_{j,t}^2)^{1/2} > R_{CA} \quad (3.1)$$

where  $R_{CA}$  is defined on an event-by-event basis as discussed in Table 1. A veto can then be applied to the remaining jets in order to elucidate the colour structure of the event.

It might be anticipated that the best separation between the colour singlet and the colour octet resonance would occur by vetoing jet activity between the two top-quark jets [1]. However, this requires the top-jets to be separated by a large enough rapidity interval. Figure 1(b) shows the signal cross sections as a function of the rapidity separation and less than 10% of signal events would be retained by a rapidity cut  $\Delta y > 2$ . Fortunately, this efficiency loss can be avoided if the veto is applied to jets that lie in a *central rapidity interval*, i.e.  $|y| < 1.5$ . This choice remains sensitive to the different colour structures because colour octet resonances radiate preferentially in the forward/backward regions whereas colour singlet resonances radiate preferentially in the central region.

Using a central rapidity interval for vetoing has the added benefit that the jets are contained within the acceptance of the tracking systems of the LHC experiments. Even though the details of such criteria are beyond the scope of this study, this will be important in order to control effects from pile-up, which can be reduced by examining the in-jet track activity and determining the amount of this activity that comes from a single vertex.

The observable of interest is the gap fraction,  $f_{gap}(Q_0)$ , defined as the fraction of the events that do not have a jet (in addition to the top-quark decay products) with  $p_T > Q_0$

and  $|y| < 1.5$ , i.e.

$$f_{gap}(Q_0) = \frac{\sigma(Q_0)}{\sigma(Q_0 = 300 \text{ GeV})}. \quad (3.2)$$

Figure 2(a) shows the gap-fraction as a function of  $Q_0$  for a heavy gluon resonance predicted by PYTHIA8 and also by the matrix element generator MadGraph/MadEvent 5 [40]. The Madgraph predictions are determined for up to three partons (in addition to the  $t\bar{t}$ ) in the final state. Figure 2(b) shows the equivalent curves for a heavy photon resonance. It is clear that the PYTHIA8 and MadGraph predictions differ for each resonance by about 10% at the lowest values of  $Q_0$ . Although these theoretical predictions are significantly different from each other (we discuss the theory uncertainty further in Section 3.5), Figure 2(c) shows that the difference between the heavy gluon and heavy photon gap fractions remains sizeable in each case and this is all we need for the fidelity of our analysis. We therefore use the results obtained using PYTHIA8 in the following sections to determine the sensitivity of the LHC experiments to the colour charge of new resonances.

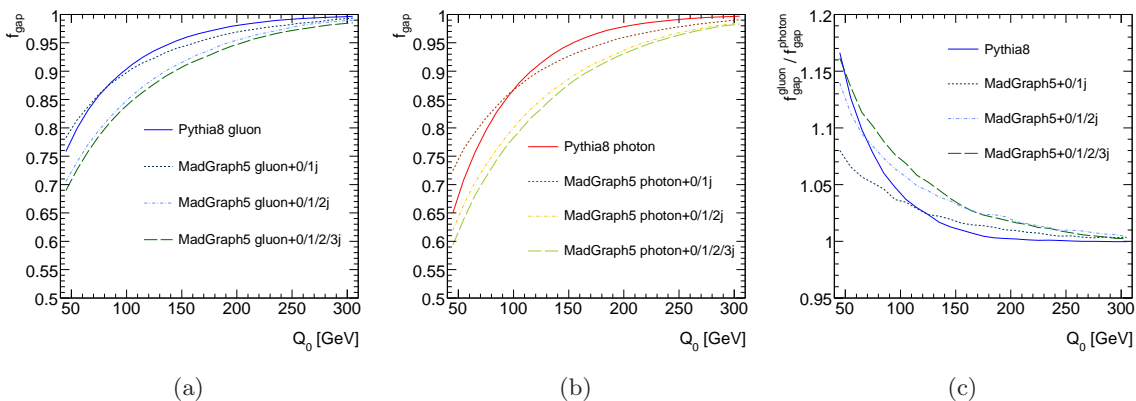


**Figure 2.** The gap-fraction for heavy gluon (a) and heavy photon (b) resonances predicted by PYTHIA8 and MadGraph. The Madgraph curves correspond to 1,2 or 3 extra partons. (c) The ratio of gluon and photon gap-fractions predicted by PYTHIA8 and MadGraph.

### 3.3 Extracting the signal from background

A pseudo-experiment approach is adopted in order to determine the expected sensitivity to the colour of the resonance at a given luminosity,  $L$ . For each signal or background process,  $i$ , the expected number of events is determined by  $\lambda_i = \sigma_i L$ , where  $\sigma_i$  is the process cross section. The actual number of events,  $n_i$ , that contribute to a given pseudo-experiment is determined using a Poisson distribution with mean equal to  $\lambda_i$ . The pseudo-experiment is constructed by selecting these events at random from reduced MC samples, i.e. after top-tagging.

The  $t\bar{t}$  invariant mass distribution,  $m_{t\bar{t}}$ , is constructed for several values of  $Q_0$  (i.e. after vetoing events that contain additional jets with  $p_T > Q_0$  in the rapidity interval  $|y| < 1.5$ ). From this we extract the size of the signal as a function of the veto scale for  $20 \text{ GeV} < Q_0 < 300 \text{ GeV}$ . The number of signal events at each value of  $Q_0$  is determined



by fitting the invariant mass distribution for both signal and background. The signal is parameterized by a skewed Breit-Wigner:

$$\frac{m_0^2 \Gamma^2 [a + b(m_{t\bar{t}} - m_0)]}{(m_{t\bar{t}}^2 - m_0^2)^2 - m_0^2 \Gamma^2} \quad (3.3)$$

and  $m_0$ ,  $\Gamma$ ,  $a$  and  $b$  are allowed to vary in the fit. The background is assumed to have a shape determined by the  $t\bar{t}$  sample and only its normalization is allowed to vary in the fit. Using just the  $t\bar{t}$  background is reasonable since the light-quark background has a very similar shape at large invariant masses. Moreover, we have examined in detail what happens if we allow the shape of the background fit to vary whilst keeping the shape of the true background unchanged: Our final results are very insensitive to even quite large changes in this shape and we are in any case confident that an experimental analysis could reliably extract the signal cross section from background. After fitting the invariant mass distribution, the number of signal events is given by  $N_s = N_T - N_b$ , where  $N_T$  is the total number of events in the pseudo-experiment that satisfy  $1.5 \text{ TeV} \leq m_{t\bar{t}} < 2.5 \text{ TeV}$  and  $N_b$  is the corresponding number of background events in this range, as extracted from the fit. The size and location of this mass window would, of course, be optimized in any analysis.

The gap-fraction as a function of  $Q_0$  for the signal events can be constructed by

$$f_{gap}(Q_0) = \frac{N_s(Q_0)}{N_s(Q_0 = 300 \text{ GeV})}. \quad (3.4)$$

Figure 3(a) shows the result of a typical pseudo-experiment in the case of a heavy gluon signal and assuming an integrated luminosity of  $10 \text{ fb}^{-1}$ . The pseudo-data are compared to the theoretical predictions (solid lines, PYTHIA8) for the heavy gluon and heavy photon cases. Although there are sizable statistical fluctuations in the pseudo-data<sup>4</sup>, it is clear that they are better represented by the heavy gluon prediction.

Our ability to extract the signal correctly is confirmed in Figure 3(b). Here the gap fraction is obtained by computing the mean across all pseudo-experiments. We clearly see that the mean gap fractions agree well with the signal-only theoretical predictions for both heavy gluon and heavy photon cases. The error bars represent the RMS spread of  $f_{gap}$  values and indicate that the gap fraction could have significant discriminating power with as little as  $10 \text{ fb}^{-1}$  of data provided the production rates are not much smaller than we are assuming.

### 3.4 Extracting the colour

The colour of the resonance can be obtained using a fit of the form

$$f_{gap}(Q_0) = a_1 f_1(Q_0) + a_8 f_8(Q_0) \quad (3.5)$$

where  $f_1$  ( $f_8$ ) is the pure theory prediction for a colour singlet (octet) resonance and the  $a_i$  are constants that are allowed to vary in the fit to data<sup>5</sup>. Figure 4(a) shows the probability

---

<sup>4</sup>The errors shown in Figure 3(a) correspond to treating the numerator and denominator in Eq. (3.4) as uncorrelated, Poisson, random values.

<sup>5</sup>We constrain them to be positive.

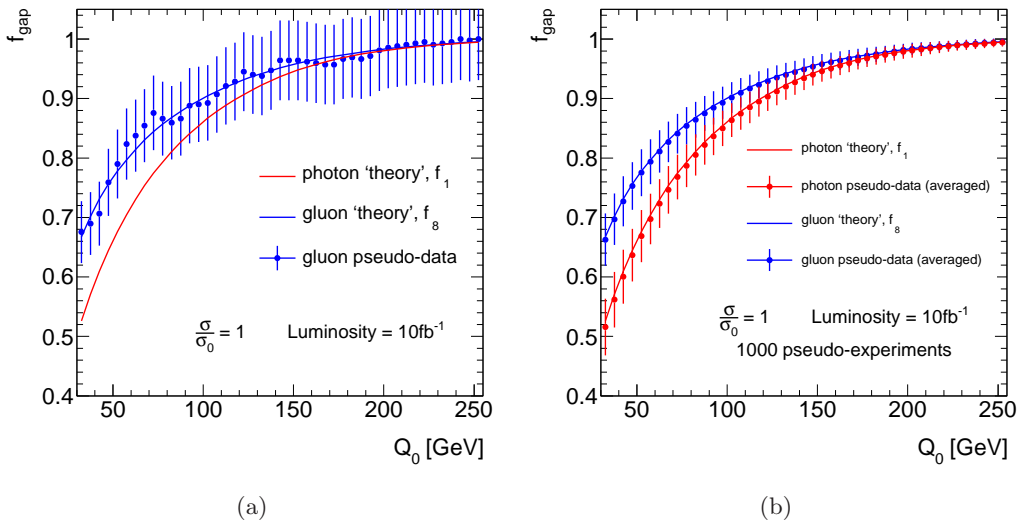


**Figure 3.** (a) The data points show the gap fraction in a typical pseudo-experiment for the case of a heavy gluon. The curves show the corresponding theoretical predictions for both a heavy photon and a heavy gluon; (b) Mean gap fraction obtained after averaging across 1000 pseudo-experiments. The errors in (b) represent the RMS spread of values obtained in the pseudo-experiments.

of obtaining a specific value of  $a_8$  for a heavy gluon signal,  $P(a_8|g)$ , assuming an integrated luminosity of  $10 \text{ fb}^{-1}$ .  $P(a_8|g)$  is strongly peaked at unity, indicating that the gluon is identified as such in the majority of pseudo-experiments. Also shown is  $P(a_1|g)$  and, as expected, it is strongly peaked at zero<sup>6</sup>. Figure 4(b) shows the corresponding distributions when the true signal is a heavy photon, i.e.  $P(a_1|\gamma)$  and  $P(a_8|\gamma)$ .

More interesting is the probability that a particular measured value of  $a_8$  is due to a gluon resonance and it can be calculated using Bayes' Theorem if we assume that prior to this analysis the resonance is equally likely to be a heavy gluon or a heavy photon:

$$P(g|a_8) = \frac{P(a_8|g)}{P(a_8|g) + P(a_8|\gamma)}. \quad (3.6)$$

Figure 5(a) shows the values of  $P(g|a_8)$  and  $P(\gamma|a_8)$  as a function of  $a_8$ . As expected,  $P(g|a_8)$  increases as  $a_8$  increases, whereas the  $P(\gamma|a_8)$  decreases. Figure 5(b) shows the values of  $P(g|a_8)$  for different values of the input luminosity.

Thus, for each pseudo-experiment a specific value of  $a_8$  can be extracted from the gap fraction fit and the probability that the resonance is a gluon (or a photon) can be determined using the probability distributions shown in Figure 5: Exactly the same procedure could be used with real data. To quantify the feasibility of making such a measurement at the LHC, we calculate the fraction of pseudo-experiments that have  $P(g|a_8)$  larger than 95%, which we denote  $G_{95}$ . For example,  $G_{95} = 0.77$  for the baseline heavy gluon signal and  $10 \text{ fb}^{-1}$  of integrated luminosity. It is very likely, therefore, that the LHC experiments could identify the colour structure of such a resonance, should it occur in Nature.

<sup>6</sup>We observe that  $a_1 + a_8 \approx 1.0$  with an RMS variation of less than 2%

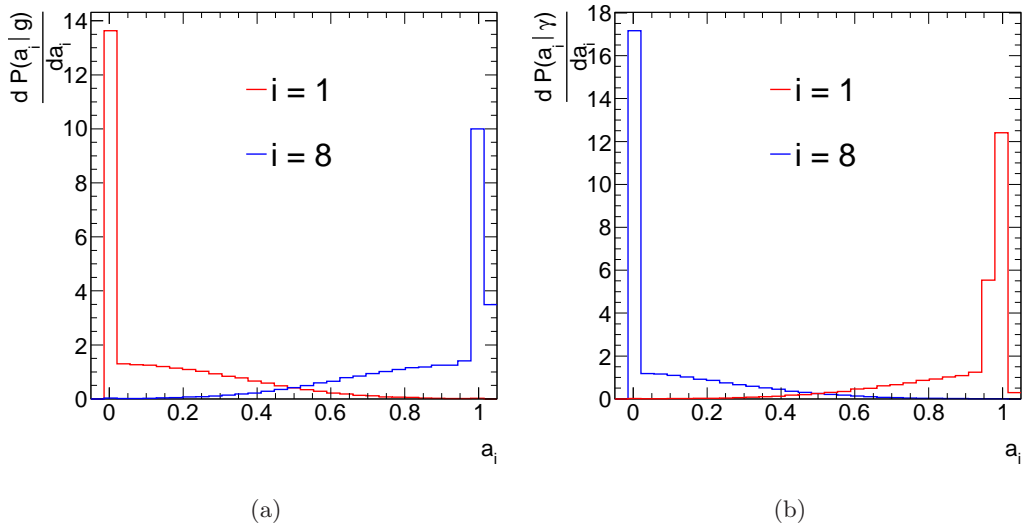


**Figure 4.** (a)  $P(a_1|g)$  and  $P(a_8|g)$  obtained from  $10^5$  pseudo-experiments for the case of a heavy gluon resonance. (b)  $P(a_1|\gamma)$  and  $P(a_8|\gamma)$  obtained from  $10^5$  pseudo-experiments for the case of a heavy photon resonance. Assuming  $10 \text{ fb}^{-1}$  of data.

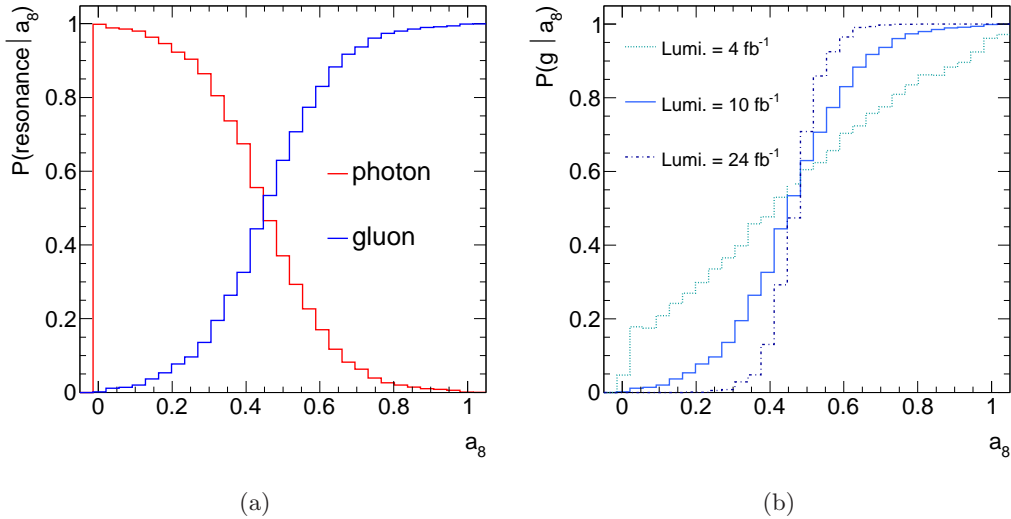


**Figure 5.** (a)  $P(g|a_8)$  and  $P(\gamma|a_8)$  in the case of a heavy gluon resonance and assuming the baseline signal size and  $10 \text{ fb}^{-1}$  of integrated luminosity. (b)  $P(g|a_8)$  for three different values of the luminosity.

In Figure 6(a) we show how  $G_{95}$  varies as we vary the size of the signal cross section relative to the baseline value ( $\sigma_0$ ) and for different integrated luminosities. For signal cross sections less than around  $1/3$  of the baseline value, a luminosity in excess of  $50 \text{ fb}^{-1}$  will be needed in order to extract the colour the resonance. Figure 6(b) shows the equivalent distribution but now for a heavy photon resonance ( $\Gamma_{95}$ ). Figure 7 shows the corresponding plots when the probability per pseudo-experiment is increased to 99% ( $G_{99}$  and  $\Gamma_{99}$ ) and

it is encouraging to note that the plots look rather similar to the previous case.

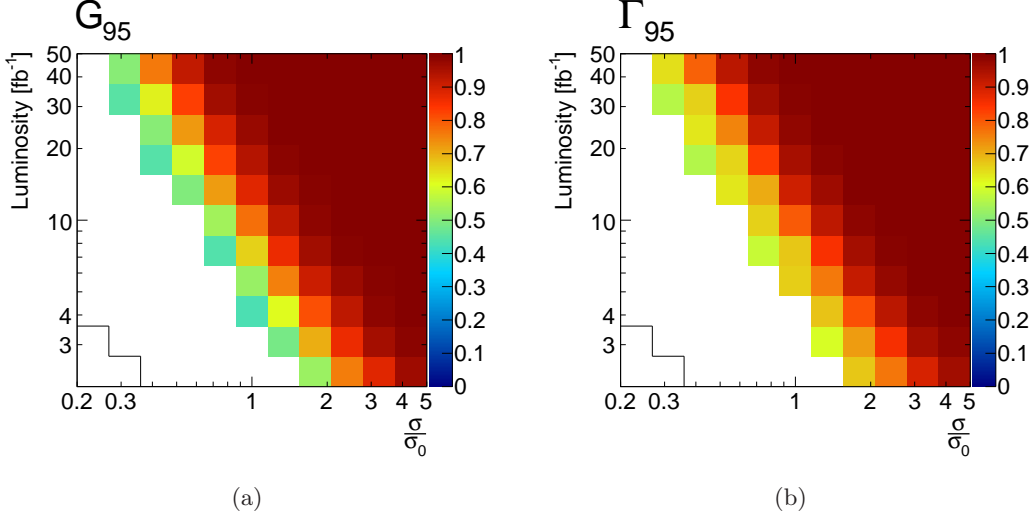


**Figure 6.** The fraction of LHC experiments that would measure  $P(g|a_8) \geq 95\%$  is denoted by  $G_{95}$ : (a)  $G_{95}$  as a function of the luminosity and signal size assuming a heavy gluon resonance. The fraction of LHC experiments that would measure  $P(\gamma|a_1) \geq 95\%$  is denoted by  $\Gamma_{95}$ : (b)  $\Gamma_{95}$  as a function of the luminosity and signal size assuming a heavy photon resonance. The solid line in the bottom left corner indicates the region where the significance of any signal is less than  $5\sigma$  significance.

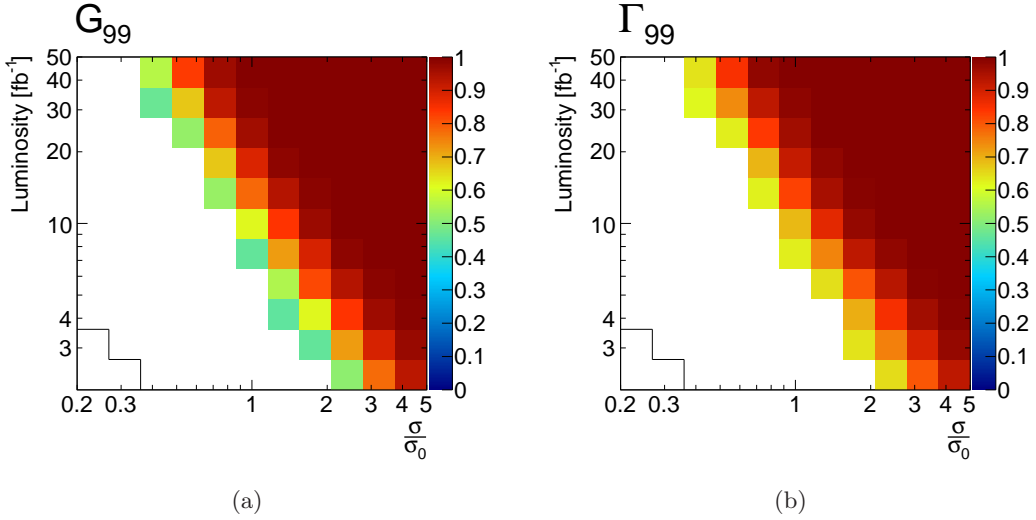


**Figure 7.** The fraction of LHC experiments that would measure  $P(g|a_8) \geq 99\%$  is denoted by  $G_{99}$ : (a)  $G_{99}$  as a function of the luminosity and signal size assuming a heavy gluon resonance. The fraction of LHC experiments that would measure  $P(\gamma|a_1) \geq 99\%$  is denoted by  $\Gamma_{99}$ : (b)  $\Gamma_{99}$  as a function of the luminosity and signal size assuming a heavy photon resonance. The solid line in the bottom left corner indicates the region where the significance of any signal is less than  $5\sigma$  significance.

### 3.5 Effect of experimental and theoretical uncertainties

Experimental and theoretical uncertainties will obviously affect our ability to determine the colour of the resonance. The experimental uncertainties associated with the extraction of the signal will, to a large extent, cancel in the ratio and so will not affect the measurement in a significant way. These include the top-tagging efficiency, luminosity and energy scale/resolution of the top-tagged jets. However, the uncertainties associated with the veto jets, i.e. the jet energy scale, jet energy resolution and jet reconstruction efficiency, do affect our ability to make the measurement. A feel for the likely systematic uncertainty from the experiment can be obtained using the ATLAS measurement of dijet production with a veto on additional central jet activity [6]. In particular, the total systematic uncertainty on the  $f_{gap}(Q_0)$  distributions were at worst 5% for  $Q_0 = 20$  GeV for dijet systems constructed from central high- $p_T$  jets.

The current theoretical uncertainties are probably much larger than this. For example, the theory predictions in [6] deviate from the ATLAS dijet data by  $\sim 25\%$  at  $Q_0 = 20$  GeV and in [41] the uncertainty in the theoretical prediction of the gap fraction was found to be approaching 50% in some regions of phase space. There is no reason to suppose that jet vetoing in boosted  $t\bar{t}$  production is much better understood. Indeed, the difference between Madgraph and PYTHIA8 was shown in Section 3.2 to be about 10%. It is clear, therefore, that the theoretical uncertainties are the limiting factor in the feasibility of making this measurement.

We quantify the impact of the theory uncertainty by arbitrarily changing the shape of the theoretical predictions used to fit the pseudo-data (i.e.  $f_1$  and  $f_8$ ). In each pseudo-experiment, we choose two uniformly distributed random numbers in the interval  $[-X, +X]$ , which give the fractional shifts that are applied to  $f_1$  and  $f_8$  at  $Q_0 = 20$  GeV. The shift of each gap fraction at  $Q_0 = 300$  GeV is by definition zero and for  $Q_0$  values between 20 GeV and 300 GeV the shift is obtained by a linear interpolation. Figure 8 shows  $G_{95}$  for  $X = 10\%$  and  $25\%$  and an uncertainty in the gap fraction at the 25% level clearly has a major impact on the measurement. Encouragingly, an overall 10% uncertainty does not degrade the measurement much. It is therefore clear that the theoretical uncertainty should be reduced to around the 10% level in order to be confident of using jet vetoing as a tool to extract the colour of heavy TeV-scale resonances.

## 4 Acknowledgments

We would like to thank Phil Bull and Christina Smith, for their insights on top-tagging, and Johan Alwall for help with Madgraph. This work was funded in the UK by STFC and in part by the EU Marie Curie Research Training Network “MCnet”, under contract number MRTN-CT-2006-035606. JC would like to acknowledge the support received for this work from the Muir Wood Award Fund granted by Peterhouse in Cambridge.

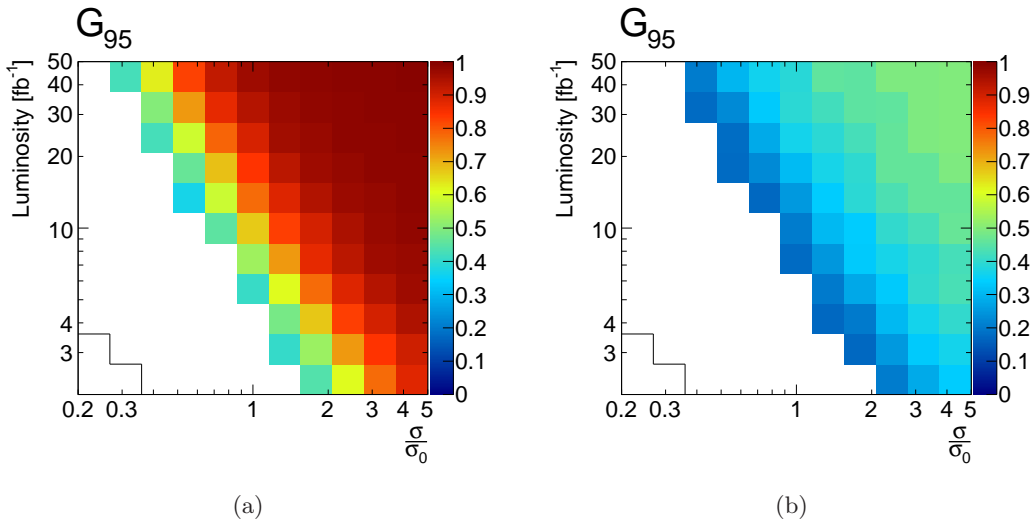


**Figure 8.** (a) The impact of a 10% uncertainty in the gap fraction shape on the value of  $G_{95}$ . (b) The impact of a 25% uncertainty in the gap fraction shape on the value of  $G_{95}$ .

## References

- [1] I. Sung, *Probing the Gauge Content of Heavy Resonances with Soft Radiation*, *Phys.Rev.* **D80** (2009) 094020, [[arXiv:0908.3688](#)].
- [2] J. Gallicchio and M. D. Schwartz, *Seeing in Color: Jet Superstructure*, *Phys. Rev. Lett.* **105** (2010) 022001, [[arXiv:1001.5027](#)].
- [3] T. Han, I. Lewis, and Z. Liu, *Colored Resonant Signals at the LHC: Largest Rate and Simplest Topology*, *JHEP* **12** (2010) 085, [[arXiv:1010.4309](#)].
- [4] C. Englert, T. Plehn, P. Schichtel, and S. Schumann, *Jets plus Missing Energy with an Autofocus*, *Phys. Rev.* **D83** (2011) 095009, [[arXiv:1102.4615](#)].
- [5] B. E. Cox, J. R. Forshaw, and A. D. Pilkington, *Extracting Higgs boson couplings using a jet veto*, *Phys.Lett.* **B696** (2011) 87–91, [[arXiv:1006.0986](#)].
- [6] **ATLAS** Collaboration, G. Aad *et. al.*, *Measurement of dijet production with a veto on additional central jet activity in  $pp$  collisions at  $\sqrt{s} = 7$  TeV using the ATLAS detector*, [arXiv:1107.1641](#).
- [7] E. Gerwick, T. Plehn, and S. Schumann, *Understanding Jet Scaling and Jet Vetos in Higgs Searches*, [arXiv:1108.3335](#).
- [8] L. Randall and R. Sundrum, *A Large mass hierarchy from a small extra dimension*, *Phys.Rev.Lett.* **83** (1999) 3370–3373, [[hep-ph/9905221](#)].
- [9] B. Lillie, L. Randall, and L.-T. Wang, *The Bulk RS KK-gluon at the LHC*, *JHEP* **0709** (2007) 074, [[hep-ph/0701166](#)].
- [10] K. Agashe, A. Belyaev, T. Krupovnickas, G. Perez, and J. Virzi, *LHC Signals from Warped Extra Dimensions*, *Phys.Rev.* **D77** (2008) 015003, [[hep-ph/0612015](#)].
- [11] Y. Grossman and M. Neubert, *Neutrino masses and mixings in nonfactorizable geometry*, *Phys.Lett.* **B474** (2000) 361–371, [[hep-ph/9912408](#)].

- [12] T. Gherghetta and A. Pomarol, *Bulk fields and supersymmetry in a slice of AdS*, *Nucl.Phys.* **B586** (2000) 141–162, [[hep-ph/0003129](#)].
- [13] S. J. Huber and Q. Shafi, *Fermion masses, mixings and proton decay in a Randall-Sundrum model*, *Phys.Lett.* **B498** (2001) 256–262, [[hep-ph/0010195](#)].
- [14] L. Randall and M. D. Schwartz, *Quantum field theory and unification in AdS5*, *JHEP* **0111** (2001) 003, [[hep-th/0108114](#)].
- [15] K. Agashe, A. Delgado, and R. Sundrum, *Grand unification in RS1*, *Annals Phys.* **304** (2003) 145–164, [[hep-ph/0212028](#)].
- [16] M. S. Carena, A. Delgado, E. Ponton, T. M. Tait, and C. Wagner, *Precision electroweak data and unification of couplings in warped extra dimensions*, *Phys.Rev.* **D68** (2003) 035010, [[hep-ph/0305188](#)].
- [17] K. Agashe, R. Contino, and R. Sundrum, *Top compositeness and precision unification*, *Phys.Rev.Lett.* **95** (2005) 171804, [[hep-ph/0502222](#)].
- [18] K. Agashe and G. Servant, *Warped unification, proton stability and dark matter*, *Phys.Rev.Lett.* **93** (2004) 231805, [[hep-ph/0403143](#)].
- [19] K. Agashe and G. Servant, *Baryon number in warped GUTs: Model building and (dark matter related) phenomenology*, *JCAP* **0502** (2005) 002, [[hep-ph/0411254](#)].
- [20] CDF Collaboration, T. Aaltonen *et. al.*, *Evidence for a Mass Dependent Forward-Backward Asymmetry in Top Quark Pair Production*, *Phys. Rev.* **D83** (2011) 112003, [[arXiv:1101.0034](#)].
- [21] CDF Collaboration, T. Aaltonen *et. al.*, *Forward-Backward Asymmetry in Top Quark Production in  $p\bar{p}$  Collisions at  $\sqrt{s} = 1.96$  TeV*, *Phys. Rev. Lett.* **101** (2008) 202001, [[arXiv:0806.2472](#)].
- [22] DØ Collaboration, V. M. Abazov *et. al.*, *Forward-backward asymmetry in top quark-antiquark production*, [arXiv:1107.4995](#).
- [23] DØ Collaboration, V. M. Abazov *et. al.*, *First measurement of the forward-backward charge asymmetry in top quark pair production*, *Phys. Rev. Lett.* **100** (2008) 142002, [[arXiv:0712.0851](#)].
- [24] Y. Bai, J. L. Hewett, J. Kaplan, and T. G. Rizzo, *LHC Predictions from a Tevatron Anomaly in the Top Quark Forward-Backward Asymmetry*, *JHEP* **03** (2011) 003, [[arXiv:1101.5203](#)].
- [25] T. Sjöstrand, S. Mrenna, and P. Z. Skands, *A Brief Introduction to PYTHIA 8.1*, *Comput.Phys.Commun.* **178** (2008) 852–867, [[arXiv:0710.3820](#)].
- [26] T. Sjöstrand, S. Mrenna, and P. Z. Skands, *PYTHIA 6.4 Physics and Manual*, *JHEP* **0605** (2006) 026, [[hep-ph/0603175](#)].
- [27] L. D. Landau *Dokl. Akad. Nauk. USSR* **60** (1948) 207.
- [28] C.-N. Yang, *Selection Rules for the Dematerialization of a Particle Into Two Photons*, *Phys.Rev.* **77** (1950) 242–245.
- [29] B. C. Allanach, F. Mahmoudi, J. P. Skittrall, and K. Sridhar, *Gluon-initiated production of a Kaluza-Klein gluon in a Bulk Randall-Sundrum model*, *JHEP* **1003** (2010) 014, [[arXiv:0910.1350](#)].
- [30] A. Djouadi, G. Moreau, F. Richard, and R. K. Singh, *The Forward-backward asymmetry of*

- top quark production at the Tevatron in warped extra dimensional models*, *Phys.Rev.* **D82** (2010) 071702, [[arXiv:0906.0604](#)].
- [31] P. Ferrario and G. Rodrigo, *Constraining heavy colored resonances from top-antitop quark events*, *Phys.Rev.* **D80** (2009) 051701, [[arXiv:0906.5541](#)].
- [32] M. Bauer, F. Goertz, U. Haisch, T. Pfoh, and S. Westhoff, *Top-Quark Forward-Backward Asymmetry in Randall-Sundrum Models Beyond the Leading Order*, *JHEP* **1011** (2010) 039, [[arXiv:1008.0742](#)].
- [33] H. Davoudiasl, J. Hewett, and T. Rizzo, *Experimental probes of localized gravity: On and off the wall*, *Phys.Rev.* **D63** (2001) 075004, [[hep-ph/0006041](#)].
- [34] **CTEQ** Collaboration, H. L. Lai *et. al.*, *Global QCD analysis of parton structure of the nucleon: CTEQ5 parton distributions*, *Eur. Phys. J.* **C12** (2000) 375–392, [[hep-ph/9903282](#)].
- [35] M. Cacciari, G. P. Salam, and G. Soyez, *The anti- $k_t$  jet clustering algorithm*, *JHEP* **04** (2008) 063, [[arXiv:0802.1189](#)].
- [36] M. Cacciari and G. P. Salam, *Dispelling the  $N^3$  myth for the  $k_t$  jet-finder*, *Phys. Lett.* **B641** (2006) 57–61, [[hep-ph/0512210](#)].
- [37] M. Cacciari, G. P. Salam, and G. Soyez. <http://fastjet.fr>.
- [38] D. E. Kaplan, K. Rehermann, M. D. Schwartz, and B. Tweedie, *Top Tagging: A Method for Identifying Boosted Hadronically Decaying Top Quarks*, *Phys. Rev. Lett.* **101** (2008) 142001, [[arXiv:0806.0848](#)].
- [39] A. Abdesselam, E. Kuutmann, U. Bitenc, G. Brooijmans, J. Butterworth, *et. al.*, *Boosted objects: A Probe of beyond the Standard Model physics*, *Eur.Phys.J.* **C71** (2011) 1661, [[arXiv:1012.5412](#)].
- [40] J. Alwall, M. Herquet, F. Maltoni, O. Mattelaer, and T. Stelzer, *MadGraph 5: Going Beyond*, *JHEP* **06** (2011) 128, [[arXiv:1106.0522](#)].
- [41] R. M. D. Delgado, J. R. Forshaw, S. Marzani, and M. H. Seymour, *The dijet cross section with a jet veto*, [arXiv:1107.2084](#).
- [42] B. Lillie, J. Shu, and T. M. Tait, *Kaluza-Klein Gluons as a Diagnostic of Warped Models*, *Phys.Rev.* **D76** (2007) 115016, [[arXiv:0706.3960](#)].

## A Appendix

This appendix highlights some of the features of the heavy gluon implementation in PYTHIA8. In particular we take a look at the strong enhancement of the  $t\bar{t}$  invariant mass distribution at low masses due to parton distribution function (PDF) effects, the potentially large interference effects that can occur between the signal and background and the forward-backward asymmetry that can be induced by non-chirally symmetry couplings of the heavy gluon to quarks.

For this appendix only, we take as our reference the typical RS couplings:  $g_L^q = g_R^q = g_R^b = -0.2$ ,  $g_L^b = g_L^t = 1$ ,  $g_R^t = 4$  [9]. These contain a significant axial-vector coupling to tops<sup>7</sup>. In the following, we do also vary the couplings about these reference values. Also

---

<sup>7</sup>We define  $g_v = (g_L + g_R)/2$  and  $g_a = (g_L - g_R)/2$ .



for this appendix only, when we speak of the  $t\bar{t}$  mass we refer to the invariant mass of the top pair at parton level, *i.e.* before showering and hadronisation.

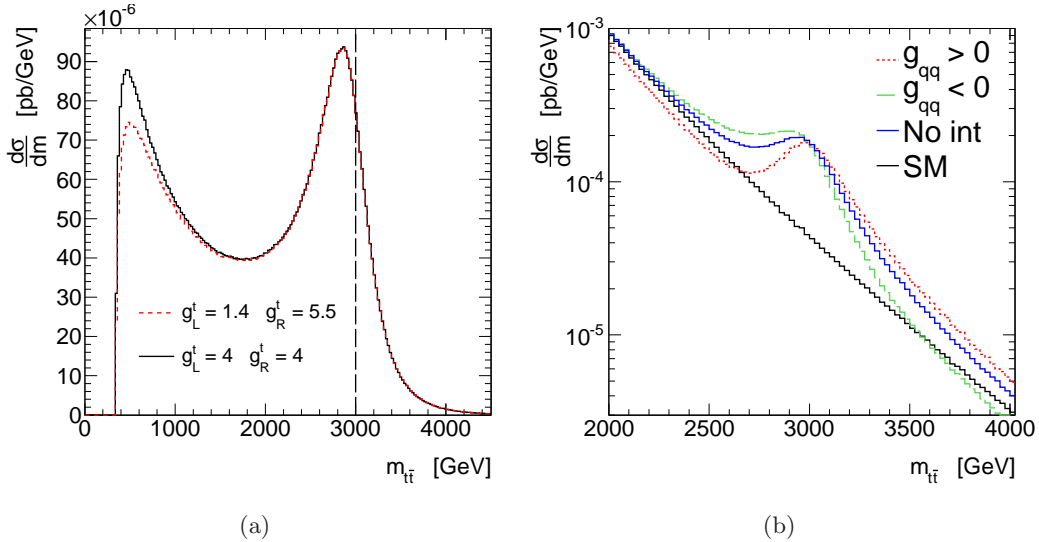


**Figure 9.** (a) Invariant  $t\bar{t}$  mass distribution for a broad gluon resonance, neglecting the SM contribution. (b) Comparison of  $t\bar{t}$  invariant mass distributions for several RS-like scenarios. Contributions from heavy and SM gluon production are included, both from  $q\bar{q}$  annihilation and gluon fusion processes. The details are explained in the text.

The first point of note is that the shape of a wide resonance can be very strongly distorted by the PDFs of the incoming particles. The fast increase of the PDFs with decreasing  $x$  competes with the suppression from the heavy gluon virtuality, enhancing the low mass tail of the resonance and suppressing it at high masses. This is illustrated in Figure 9(a), which shows the  $t\bar{t}$  mass spectrum for the ‘pure’ heavy gluon process (*i.e.* without any SM background or interference effects) for a wide resonance with  $m_{\tilde{G}} = 3$  TeV,  $g_v^t = 4$  and  $g_a^t = 0$ . The shift of the peak can be significant for large resonance mass and couplings, but tends not to be larger than about 100 GeV for typical RS scenarios that might be seen at the LHC. Similarly, large mass and couplings also imply that a large fraction of the resonance cross section resides in the low mass tail and this fraction is sensitive to the choice of mass and couplings. It should also be noted that the tail fraction can be significant even for a relatively light resonance and that it is quite possible to encounter scenarios where only the minority of the cross section resides in the resonance peak. Figure 9(a) also demonstrates the small difference introduced by adding some axial coupling while maintaining the same overall normalisation ( $g_v^t = 3.45$ ,  $g_a^t = 2.05$ ). It can be seen that while the balance of axial and vector couplings does have some effect on the low mass tail of the  $t\bar{t}$  mass spectrum, its effect on the main part of the resonance peak is very small.

While most of the SM  $t\bar{t}$  events at the LHC are initiated by gluon fusion, a significant fraction comes from quark annihilation, which can interfere with the heavy gluon amplitude. The nature of this interference is sensitive to the model parameters and so, in principle,

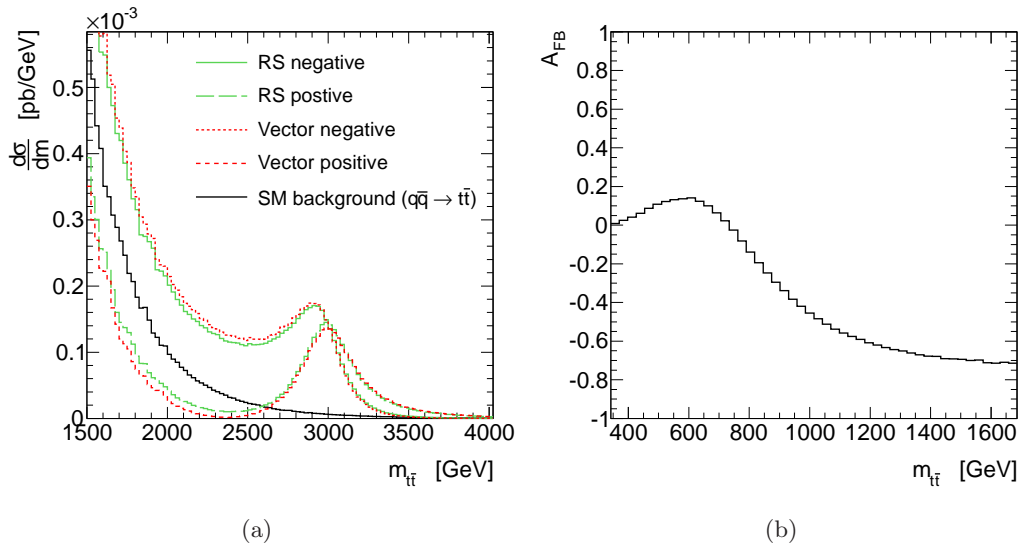


**Figure 10.** (a) Comparison of invariant  $t\bar{t}$  mass distributions for RS-like and vector coupling scenarios. Contributions from both heavy and SM gluon production are included, but only from  $q\bar{q}$  annihilation. (b) Forward-backward asymmetry as a function of the  $t\bar{t}$  invariant mass. The details are explained in the text.

could be used to constrain the heavy gluon. Note that the interference changes sign at the  $\tilde{G}$  mass: RS models typically predict a negative coupling to the incoming light quarks and a positive coupling to the outgoing top quarks, which would result in constructive interference below the resonance peak and destructive interference above. This would be reversed if the couplings to the incoming and outgoing quarks were of the same sign. Figure 9(b) compares the  $t\bar{t}$  mass spectrum for the typical RS scenario ( $g_{qq} < 0$ ) to an equivalent scenario with only positive couplings ( $g_{qq} > 0$ ) and also to the situation where interference effects are not taken into account (“No int”). As pointed out, for example in [42], this shows that interference effects can certainly be significant, even on top of the full SM  $t\bar{t}$  background. We can say a little more about how the strength of the interference depends on the balance of axial and vector top couplings: Since only the vector part of the heavy gluon coupling interferes with the SM background it is to be expected that reducing the vector coupling and increasing axial coupling will reduce the strength of the interference. Figure 10(a), which compares the RS scenario with interference that was used to produce Figure 9(b) ( $g_v^t = 2.5, g_a^t = 1.5$ ) to its purely vector coupling equivalent ( $g_v^t = 2.92, g_a^t = 0$ ), demonstrates that this difference is small when comparing RS-like to vector scenarios and it will be quite negligible once the gluon fusion background is added in (it is not included in the figure for clarity).

To conclude this appendix, we take a look at the forward-backward asymmetry for  $p\bar{p}$  collisions at  $\sqrt{s} = 1.96$  TeV. Here we can make direct comparisons with results in the literature in order to validate our implementation. Two different sets of parameters were considered:

- $m_{\tilde{G}} = 2.75$  TeV,  $g_L^q = 4.5$ ,  $g_R^q = -0.2$ ,  $g_R^b = 2$ ,  $g_L^b = g_L^t = 0$  and  $g_R^t = 6.1$  based on

[30];

- $m_{\tilde{G}} = 1.0$  TeV,  $g_v^q = g_v^b = g_v^t = 0$  and  $g_a^q = -g_a^b = -g_a^t = 1$  based on [31].

For the heavy gluon contribution to the asymmetry, we find  $A_{FB} = 0.05$  and  $A_{FB} = 0.14$  respectively (at parton level), which agree with the published results. Figure 10(b) shows  $A_{FB}$  as a function of the invariant mass of the top pair, using the parameter set from [30]. We note that the asymmetry correctly passes through zero at  $m_{t\bar{t}} = m_{\tilde{G}}/\sqrt{1 + 2g_v^q g_v^t}$ .